



Cite this: *Phys. Chem. Chem. Phys.*,
2025, **27**, 19379

Molecular dynamics of space-confined water inside Span 80 reverse micelles with an all-atom and coarse-grained solvent

Andrea Piserchia, Sergio Rampino, * Mirco Zerbetto, Francesca Tajoli, Silvia Gross and Antonino Polimeno

We investigate the structural and dynamical properties of confined water in reverse micelles (RMs) by means of molecular dynamics simulations and we assess the effect of coarse-grained (CG) modeling of the solvent on their reproducibility. In particular, simulations of three differently-sized RMs constituted by Span 80 (sorbitan monooleate) surfactant molecules dispersed in cyclohexane solvent ('oil phase') were set up by varying the number of surfactant molecules and the water-to-surfactant ratio. The resulting RMs have a number of Span 80 molecules equal to 51, 246, and 475, respectively, and average inner-core water radii in the range of 10–60 Å. For the oil phase, three different levels of description of the cyclohexane molecules are considered: an all-atom (AA) description and two different CG versions constituted by three and two beads, respectively, where each bead interacts with other beads and atoms *via* a standard Lennard-Jones 12-6 potential. All simulations were performed with the NAMD package. Our results highlight the presence of two distinct regions of inner-core and interfacial water, and show that the structural and dynamical properties of these are not significantly affected by a CG modeling of cyclohexane, confirming that the simulation time can be considerably reduced by blurring the solvent details while keeping an accurate AA description of the part of the system of real interest.

Received 3rd July 2025,
Accepted 12th August 2025

DOI: 10.1039/d5cp02542g

rsc.li/pccp

1 Introduction

Water in confined space (for example, in micelles, nanotubes, nanopores, *etc.*) exhibits deep changes in structural, dynamical, and thermodynamical properties with respect to bulk water.^{1–10} These changes depend on the degree and geometrical features of the confinement and include the lowering of the freezing point, the formation of different polymorphs, the hysteresis between freezing and melting, and the highly anisotropic orientational dynamics of water dipoles. Inorganic and organic chemical reactions occurring in confined space also differ in many aspects from those conducted in bulk solution in terms of different crystallization outcomes,¹¹ phase behavior, polymorph stability rankings, altered regioselectivity, enhanced stability, and accelerated substrate reactivity compared to bulk environments. The relevance of this topic is self-evident considering that many biological processes and transport phenomena take place in crowded aqueous surroundings.

The understanding of these phenomena is improved by a detailed description of the structure and dynamics of confined water acting as a medium for reaction and crystallization events

in spatially confined environments. For this purpose, a convenient computational approach is given by molecular dynamics (MD),¹² which can provide predictive modeling tools capable of quantitatively describing the physicochemical structural and dynamical changes that affect host molecules and the effects of nanoconfinements on chemical reactions. However, computational simulations of confined systems can be demanding, depending on the size of the system and its level of description. In particular, one of the biggest hurdles in MD simulations of reverse micelles (RMs) is the huge quantity of solvent molecules (the 'oil phase') needed in the MD simulation box, often resulting in prohibitive requirements in terms of computational resources. Typically, the oil phase occupies 70–90% of the total number of atoms in the simulation, and for the purposes of describing the properties of confined water in RMs, the apolar solvent molecules constitute a scarcely relevant but unavoidable filler that has to be included to keep the simulated RM intact.

In this context, coarse-grained (CG) modeling represents an important route to reduce the degrees of freedom involved and consequently the required computational effort, while keeping an accurate description of the structural and dynamical properties of the relevant portion of the considered systems.^{13–15} In CG approaches, the atomistic representation of the solvent is

Dipartimento di Scienze Chimiche, Università degli Studi di Padova, Via Marzolo 1, Padova, 35131, Italy. E-mail: sergio.rampino@unipd.it



replaced by a simplified description in which groups of atoms are treated as interacting beads (*i.e.*, simplified representations of a group of atoms that are treated as single interaction sites or particles in the simulation). This enables the study of larger RMs that require large quantities of solvent molecules for their simulations at reasonable computing time, preserving a particle description of the oil phase and avoiding drastic simplifications provided, for instance, by implicit solvent methods.

Several investigations have been presented based on MD simulations of space-confined water inside RMs, with particular emphasis on RMs resulting from water and the anionic surfactant sodium di(2-ethylhexyl)sulfosuccinate (also known as aerosol OT, AOT),^{16–23} due to their relevance as experimental models of space-confined microenvironments for chemical reactions, *e.g.* synthesis of polymeric and inorganic nanoparticles in miniemulsion,²⁴ and biological processes, *e.g.* protein folding in RMs.²⁵ On the other hand, nonionic surfactants have the advantage of being typically less toxic,²⁶ more biocompatible,²⁷ and biodegradable,²⁸ all characteristics particularly relevant in the food, cosmetic and pharmaceutical industries.

Few works are available, to our knowledge, on RM systems of the nonionic surfactant Span 80 (sorbitan monooleate, Fig. 1(a)),^{29–32} and they all focus on small RM systems made of 15 to 50 Span 80 molecules. In the present work, we set out to investigate by means of MD simulations, the effects on the structural and dynamical properties of water confined in considerably larger Span 80 RMs in an oil phase of cyclohexane. In particular, we focus on three pre-assembled differently sized RMs with a number of Span 80 molecules equal to 51, 246 and 475, respectively, and average inner-core water radii in the

range of 10–60 Å. We consider an all-atom (AA) and two different coarse-grained (CG) models for the solvent. While other works^{33,34} have studied the RM self-assembling process using a CG description of all the molecules involved (typically using the popular MARTINI atom-to-bead mapping and related force fields^{35,36}), we focus here on exploring the effects of a CG modeling of the solvent on the properties of confined water by comparing the results obtained using both AA and CG solvents while preserving a fully atomistic description of the RMs.

The article is organized as follows. In the methods section, details are given on the system setup, computational protocol, and simulation analysis. In the results section, the results of the simulations are presented and discussed. In the last section, conclusions are drawn and perspectives are outlined.

2 Methods

2.1 System setup

We simulated three RM systems of increasing size, which we refer to as small, S, medium, M, and large, L (see Fig. 1). These were defined by setting, in a preliminary setup phase, an initial inner-core water radius r_w^o of 10, 30, and 50 Å, respectively, and varying the number of surfactant molecules and the water-surfactant molecule ratio, $w_0 = [n_w]/[n_{\text{span80}}]$. Note that the actual inner-core water radius r_w may slightly vary during the simulation due to fluctuations and to the fact that the RMs may slightly shrink or expand upon equilibration. Each RM is pre-assembled and its initial structure is built using the Packmol software³⁷ by setting the distance tolerance equal to 2.0 Å. The packing is carried out by simultaneously constraining water

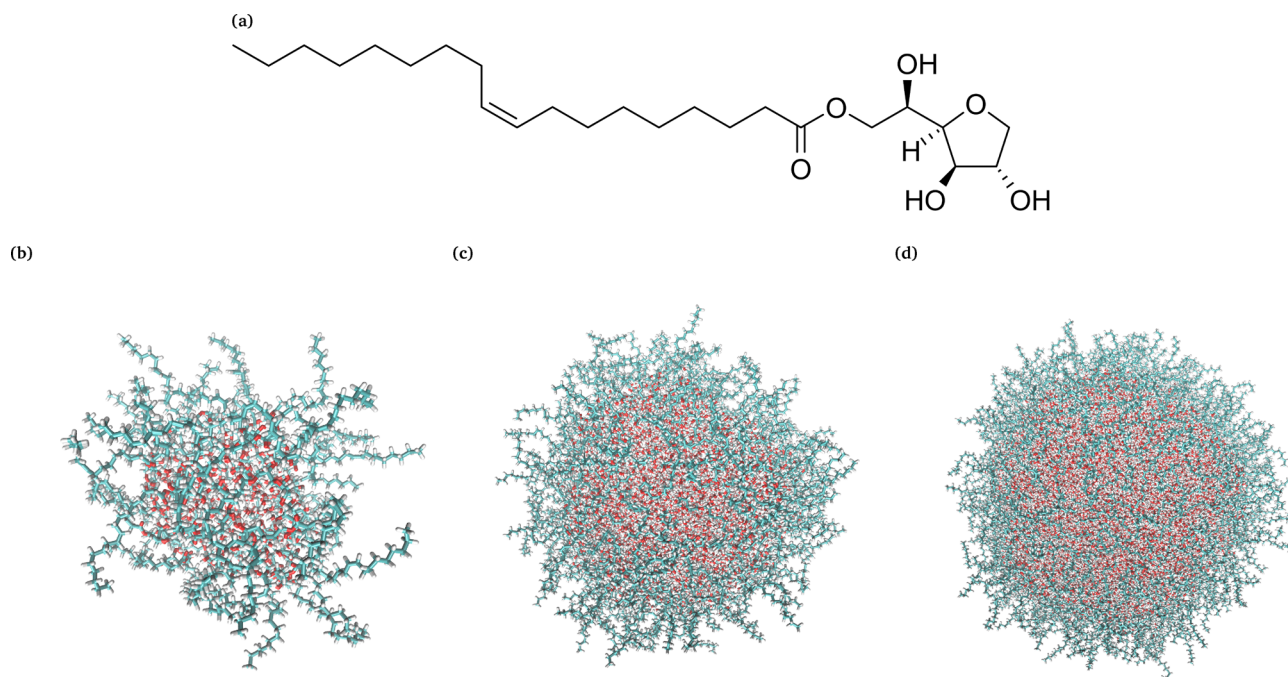


Fig. 1 Structural formula of Span 80 (a) and 3D equilibrated structures of the S (b), M (c), and L (d) RMs considered in this work. In the 3D representations of panels (b)–(d) as well as of Fig. 2 and 3, light blue color is used for carbon atoms, red color for oxygen atoms, and light gray color for hydrogen atoms.



molecules within a radius sphere r_w^o and confining Span 80 molecules to be between a spherical shell of radius $r_w^o + 2.0 \text{ \AA} < r_{\text{shell}}^o < r_w^o + 2.0 \text{ \AA} + l_{\text{Span80}}$ with their polar heads pointing towards water molecules. Here, $l_{\text{Span80}} = 27.1 \text{ \AA}$ is the length of the Span 80 chain in the all-*trans* configuration. The remaining cyclohexane molecules are packed inside the cubic simulation box with constraint $r > r_w^o + 2.0 \text{ \AA}$. For all RMs considered, the dimension of the simulation box has been chosen such that the distance between the surface of the RM and the box boundary is at least 10 \AA to avoid any short-range interaction between the periodic images.

Unlike other systems such as AOT RM,^{38,39} to our knowledge, there are no experimental data in the literature reporting the average number of water molecules (n_w) and Span 80 (n_{Span80}) at a given w_0 , so we had no direct hints on how to set realistic values for n_w and n_{Span80} . In the absence of this information, we opted for assuming the same correlation between r_w , n_w and n_{Span80} as the one reported in other experimental works on RM size determination. In particular, we chose the work of Amararene and co-workers³⁹ in which they determined the size of AOT RMs in decane by means of small angle X-ray scattering and modeled the correlation between r_w , n_w and n_{AOT} . Notice that models that estimate RM size parameters at given w_0 are present in the literature (see, for instance, ref. 40) relative to the determination of the size of the AOT RMs, but they all rely on experimental data that are missing for the systems considered in our work.

For each of the RMs considered, different levels of description for the oil phase (cyclohexane) were used. Specifically, we have considered an AA description of cyclohexane molecules and, similarly to the work of Szklarczyk *et al.*,^{41,42} two CG descriptions, the first made up of three beads (3BDS), *i.e.*, two CH_2 groups form one bead, and the second made up of two beads (2BDS), *i.e.*, three CH_2 groups form one bead (for the L system, only simulations with AA and 3BDS solvent were performed). The various levels of description for the cyclohexane molecules are sketched in Fig. 2.

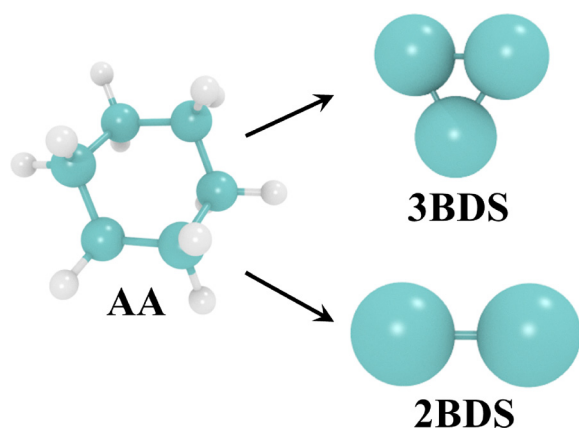


Fig. 2 Three cyclohexane models used in the RM simulations, namely the AA model and the two CG models constituted by three beads (3BDS), each one obtained by the union of two adjacent $-(\text{CH}_2)-$ groups, and two beads (2BDS), each one obtained by the union of three adjacent $-(\text{CH}_2)-$ groups.

The number of cyclohexane molecules (n_{chx}) is such that the density of cyclohexane at 300 K is reproduced. A summary of the details of each of the simulated systems is given in Table 1, where the respective total number of atoms is also reported to give an idea of the computational complexity of each simulation.

2.2 Computational details

All MD trajectories were calculated in the NpT ensemble with $p = 1 \text{ atm}$ and $T = 300 \text{ K}$ using the NAMD 2.12 package⁴³ with the CHARMM36^{44,45} AA force field for all molecules except Span 80, for which CHARMM-GUI⁴⁶ was used. This choice was dictated by the absence of AA force fields for Span 80 in the literature (only united atoms and/or MARTINI force field versions^{47,48} are available). For the CG versions of cyclohexane (3BDS, 2BDS) each bead i interacts with other beads and atoms j only *via* intermolecular interactions described by a standard Lennard-Jones 12-6 potential

$$V(r_{i,j}) = \varepsilon_{i,j} \left[\left(\frac{r_{i,j}^{\min}}{r_{i,j}} \right)^{12} - 2 \left(\frac{r_{i,j}^{\min}}{r_{i,j}} \right)^6 \right] \quad (1)$$

with $\varepsilon_{i,j}$ and $r_{i,j}^{\min}$ built using Lorentz–Berthelot rules, namely, $\varepsilon_{i,j} = \sqrt{\varepsilon_i \varepsilon_j}$ and $r_{i,j}^{\min} = \frac{r_i^{\min} + r_j^{\min}}{2}$. Lennard-Jones parameters for the beads were taken from ref. 42 (the full list of parameters can be accessed in the .par files provided as SI). A TIP3P water model⁴⁹ was used and all H-containing bonds were restricted by the SHAKE algorithm in all simulations. Periodic boundary conditions were applied in all directions. Temperature coupling was used to thermostat the system, while a Nosé-Hoover Langevin piston (piston period 200 fs, piston decay 100 fs, piston temperature equal to the thermostat temperature) was used as a barostat. Further parameters are the pair list distance set to 12 \AA , the cutoff for nonbonded interactions set to 10 \AA , with a smoothing switch at 8 \AA , and electrostatic Ewald particle mesh with tolerance set to 10^{-5} .

The MD simulation protocol for each system started with energy minimization using the conjugate gradient method to remove any clashes between the molecules. Then a gradual heating was performed from 30 K to the target temperature of 300 K, followed by an equilibration NpT of 20 ns for the stabilization of RMSD. Then, a single 20 ns long production trajectory was calculated, with a time step of integration of 2 fs. The trajectory frames were collected every 1 ps for subsequent analysis. Furthermore, we performed an NpT simulation for bulk water in a cubic box of side length equal to 50 \AA and periodic boundary conditions for comparison with RM systems by adopting the same protocol as above. Homemade scripts and VMD software⁵⁰ were used for the analysis reported in the following.

2.3 Analysis

We analyzed the whole MD run (20 ns) to investigate different structural order parameters characterizing the various RM systems and to assess the agreement between the results of the AA and CG simulations. The main focus was on the analysis



Table 1 Details of the three considered RM systems (S, M, and L) using the three levels of description (AA, 3BDS, and 2BDS) of cyclohexane molecules. r_w^o is the initial inner-core water radius; l_{box} is the side length of the cubic simulation box; n_w , n_{span80} and n_{chx} are the number of water, Span 80 and cyclohexane molecules, respectively; n_{tot} is the total number of atoms/beads involved in the simulations; t_{sim} is the approximate simulation time in h in order to run a 1 ns trajectory of a given system

	r_w^o (Å)	l_{box} (Å)	n_w	n_{span80}	n_{chx}	n_{tot}			t_{sim}^a (h ns ⁻¹)		
						AA	3BDS	2BDS	AA	3BDS	2BDS
S	10	100	153	51	4922	92 829	18 999	14 077	3.76	0.48	0.44
M	30	160	3762	246	17 692	387 834	89 214	69 306	15.27	2.36	2.15
L	50	200	12 825	475	37 272	744 521	185 441	148 169	34.79	13.92	12.05
Bulk	—	50	4111	—	—	12 333	—	—	0.29	—	—

^a Simulations performed on the Curie cluster of C3P facilities, parallelized on hybrid CPU/GPU nodes using 1 CPU AMD Opteron 6238 with 12 cores and 3 GPUs Tesla K20Xm with Infiniband.

of properties related to the inner-core water. Specifically, in line with previous MD works on RMs,^{16,19–23} we calculated:

- The radius of gyration R_g , calculated as the root-mean-square distance of the water core molecules \mathbf{r}_i from the center of mass \mathbf{r}_{com} of the RM

$$R_g = \sqrt{\frac{\sum_{i=1}^{n_w} |\mathbf{r}_i - \mathbf{r}_{\text{com}}|^2}{n_w}}; \quad (2)$$

- The eccentricity e , calculated by approximating the shape of the RM to an ellipsoid of uniform density. From the principal moments of inertia, *i.e.* the three eigenvalues of the inertia tensor, e is calculated as

$$e = 1 - \frac{I_{\text{min}}}{I_{\text{avg}}}; \quad (3)$$

where I_{min} is the lowest eigenvalue and I_{avg} the mean of the three. Eccentricity is a commonly used measure of the degree to which a shape deviates from spherical ($e = 0$ is a perfect sphere and $e \rightarrow 1$ for a flat or disc-like and rod-like shapes).

- The inner-core water radial density profiles $\rho(r)$, in order to investigate the size and the spatial extent of the molecular components of each RM and make a comparison with the bulk water density. Here r is the distance from the water core center of mass.

- The tetrahedral order parameter^{51,52} Q_i of the i th water molecule (used in different works^{53,54})

$$Q_i = 1 - \frac{3}{8} \sum_{j=1}^3 \sum_{k=j+1}^4 \left(\cos \theta_{jik} + \frac{1}{3} \right)^2 \quad (4)$$

where θ_{jik} is the angle formed by the axes joining the oxygen atom of the i th water molecule and the nearest atom of each pair (identified by indices j and k) of the four nearest neighboring molecules (Fig. 3(a)). Averaging over n_w , $Q = 1$ indicates a perfect tetrahedral packing of water molecules, while $Q \rightarrow 0$ indicates a random and uniform distribution of θ_{jik} angles;

- The number of hydrogen bonds n_{HB} , calculated with the following geometric criteria:⁵⁵ if the $r_{\text{O} \cdots \text{O}}$ distance between the donor and the acceptor atoms is less than 3.5 Å and simultaneously the absolute value of the angle between the vectors $\mathbf{r}_{\text{O-H}}$ (with O-H belonging to the donor molecule) and $r_{\text{O} \cdots \text{O}}$ (with the first oxygen atom belonging to the donor molecule and the second one to the acceptor molecule) is less than 30° (see Fig. 3(b)).

- The translational diffusion coefficient of core water D calculated from the time derivative of the mean square displacement (MSD) of water molecules (valid at large times), using Einstein's relation⁵⁶

$$D = \lim_{t \rightarrow \infty} \frac{1}{6} \frac{d\text{MSD}}{dt}. \quad (5)$$

Radial density, tetrahedral order parameter and average number of hydrogen bonds are all averaged quantities and

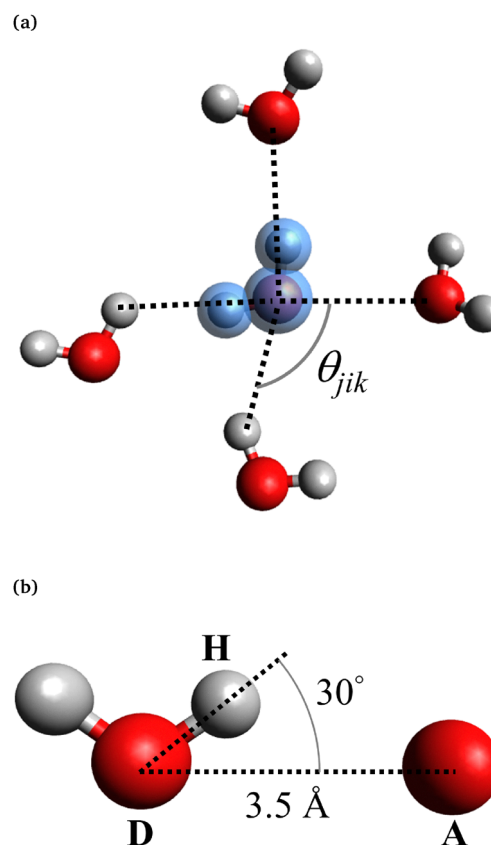


Fig. 3 Sketch of (a) tetrahedral order parameter Q calculated as in eqn (4). The generic i -th water molecule is here highlighted in pale blue and the angle subtended on its oxygen atom with a pair of four nearest neighboring molecules θ_{jik} is sketched; (b) hydrogen bond geometric criteria used in this paper: the distance between donor D, and acceptor A, oxygens must be < 3.5 Å and the angle between D–H and D···A < 30°.



are calculated and presented in a shell-wise manner, that is, consecutive concentric spherical shells are constructed around the center of mass of the water pool, each 1 Å thick, and all of the above mentioned properties are averaged for all the water molecules lying within the radial shells. Finally, in order to provide a more realistic description of interfacial water, for both the tetrahedral order parameter and the average number of hydrogen bond calculations we have also taken into account all oxygen atoms of the surfactant sorbitan moieties (*i.e.*, these atoms were included in the search for the nearest atoms to a given water molecule according to the criteria sketched in Fig. 3(a) and (b)).

3 Results and discussion

After minimization and annealing, the equilibration phase was monitored by means of RMSD stabilization. In particular, equilibrium was reached after approximately 2, 6, and 10 ns for the S, M, and L systems, respectively. During equilibration and MD production runs, few (from a minimum of one to a maximum of eight) water molecules were observed to leave the inner core of the RM and reenter the RM. This occurred for some of the considered RMs, independently of the cyclohexane level of description adopted, and no neat loss of water was observed for all of the simulated systems.

All structures remain stable and a quasi-spherical shape is preserved throughout the simulations (see Fig. 1 for snapshots of the equilibrated RMs). This is also confirmed by the time evolution of the radius of gyration of the inner-core water reported in Fig. 4 and its corresponding eccentricity reported in Fig. 5 and calculated as detailed in Section 2.3. They both present very small shape fluctuations for all systems except S, for which they are more pronounced. As both figures clearly show, the effect of the coarse graining of the solvent is practically irrelevant on these properties. The S systems feature markedly higher eccentricities (e sometimes reaching 0.5 for the AA simulation) with respect to the M and L systems

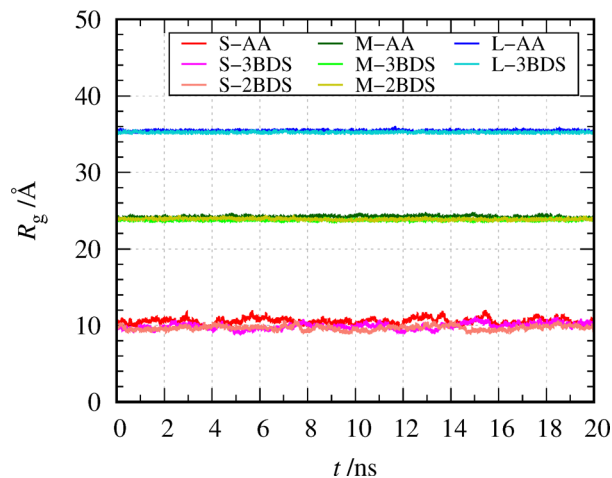


Fig. 4 Radius of gyration of the inner-core water for all the simulated RMs calculated as in eqn (2).

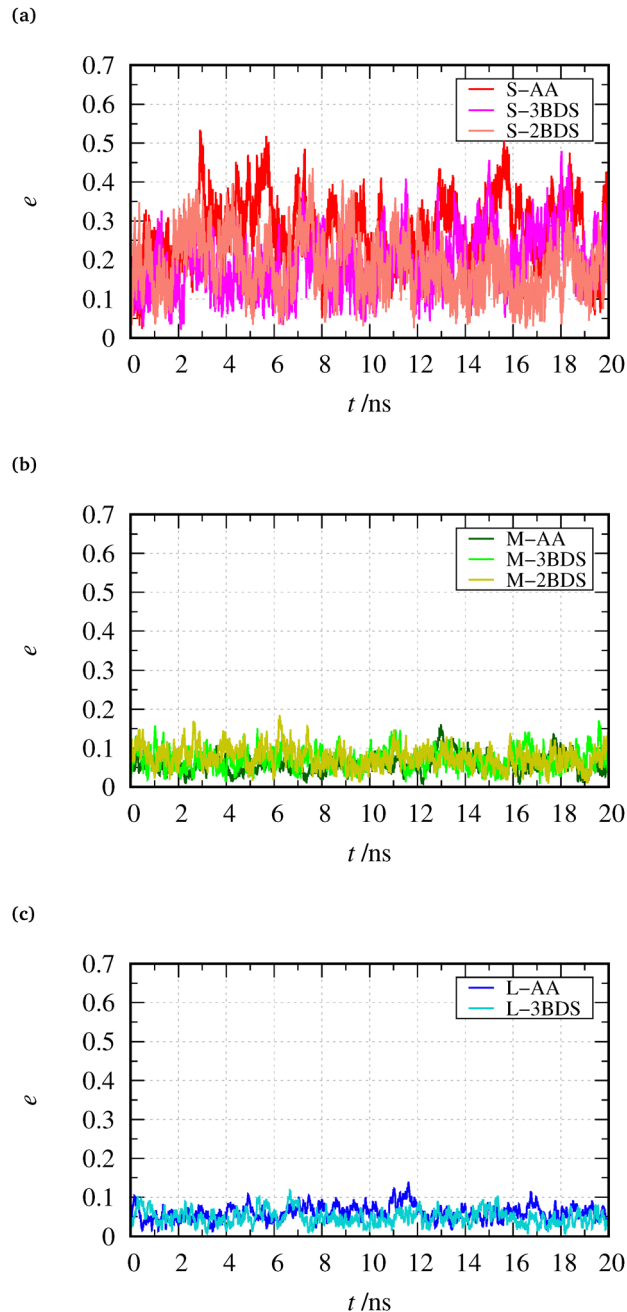


Fig. 5 Eccentricity of the inner-core water for the S (a), M (b), and L (c) simulated RMs, calculated as in eqn (3).

($e \sim 0.075$ and 0.05 , respectively), thus implying a less spheric shape in line with the results reported in ref. 30 for smaller RMs (RMs with 15 to 30 Span 80 molecules are shown there to have $e \sim 0.7$).

Fig. 6 shows the average radial density profiles calculated and presented in a shell-wise fashion as described in Section 2.3 for all the simulated RMs and for the bulk water. For all systems, the density of water is equal to that of bulk water ($\sim 1.0 \text{ g cm}^{-3}$) in the vicinity of the RM center of mass and a progressive decay is then observed when approaching the borders imposed by the polar heads of the surfactant



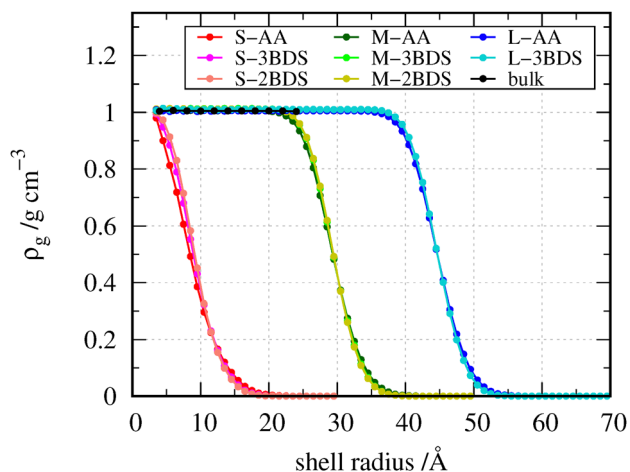


Fig. 6 Shell-wise inner-core water average radial density profiles.

molecules, until the density vanishes past this interfacial region. This evidence reflects one of the most important features imposed on water by confinement effects, that is, the separation in two distinct areas, the first one represented by bulk-like water around the RM core, while the second one represented by interfacial water that has distinctive structural and dynamical properties as compared to the bulk one. The spatial extent of the two regions depends on the size of the systems considered. In particular, for S, the average radial density profile of the water decays at about 3.5 Å and vanishes at about 20 Å, so that only a very small region at the core of the RM contains ordinary water. For M and L, on the contrary, the density profile starts decaying at about 20 Å and 35 Å, respectively, and vanishes at about 40 Å and 55 Å, respectively.

The steepness of the density drop can be assumed as a qualitative degree of this progressive change, and also can reflect an indirect measure of the effective inner-core water radius. One could eventually compare these results with SAXS experiments, but unfortunately to the best of our knowledge, there are no such experimental results in the literature for the studied RMs. It is worth noting here that the water average radial density profiles calculated with AA cyclohexane are also well reproduced by the corresponding two CG versions.

From the analysis of Fig. 4–6, it can be noticed that the S, M, and L RMs underwent either a small shrinkage or expansion with respect to the value of the initial r_w^o , consistent for all the descriptions of cyclohexane levels. We believe that this is due to the chosen water-to-surfactant ratio used that, due to lack of information, does not exactly reflect the real one for a given r_w . Also, for S the proximity of the polar heads of Span 80 molecules one with each other could result in a slight expansion of the RM itself due to steric effects.

The radial profiles of the tetrahedral order parameter Q are reported in Fig. 7. For all RM sizes, they are negligibly affected by the level of description of cyclohexane, and they all show the same trend. Starting from a bulk-like value (for the TIP3P water model) $Q \sim 0.56$ the tetrahedral order parameter starts to drop at distance values close to the same as found for the radial

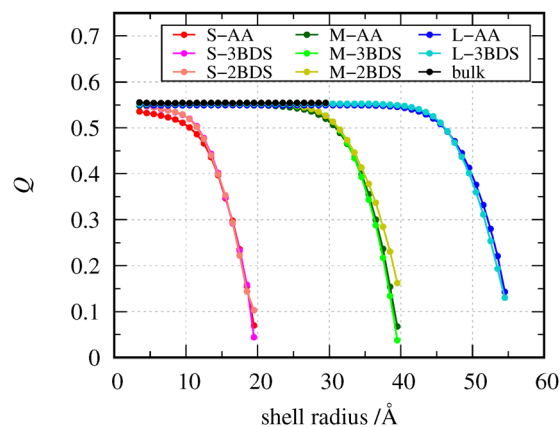


Fig. 7 Shell-wise average tetrahedral order parameter calculated as in eqn (4).

density profiles. When moving from the center towards the interfacial region, the water molecules progressively lose their tetrahedral packing because of the confinement effect. This phenomenon, as evident from the calculated profile, is absent in the bulk water (black line in Fig. 7).

The decay steepness reflects very well the one found for water in oil systems rather than the one for RMs constituted by ionic surfactant like AOT, (see Fig. 2(b) in the work of Hande and Chakrabarty²³), indicating that water properties in RMs constituted by nonionic surfactant like Span 80 are mainly due to geometric confinement rather than interactions with surfactant polar heads, while the same is not true for ionic surfactant where the charged heads affect water properties at longer range because of electrostatic interactions.²³

Fig. 8 shows the shell-wise average number of hydrogen bonds in the shell as a function of the shell radius, confirming the above outlined picture of two regions of water. For each of the systems considered, the average number of hydrogen bonds is very similar to that found in bulk water (~ 1.65) for all shells but those near the interface region, where it is seen to undergo a slight decrease consistent with all levels of the description of cyclohexane. It is worth noting here that the decrease of

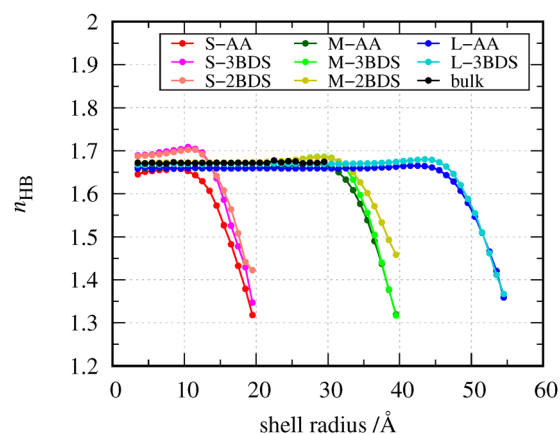


Fig. 8 Shell-wise average number of hydrogen bonds.



Table 2 Self-diffusion coefficients of water calculated from MSD, see eqn (5)

	D (cm ² s ⁻¹)		
	AA	3BDS	2BDS
S	2.03×10^{-6}	1.49×10^{-6}	1.93×10^{-6}
M	7.16×10^{-7}	1.04×10^{-7}	1.87×10^{-7}
L	7.51×10^{-6}	4.85×10^{-7}	—
Bulk	2.57×10^{-5}	—	—
Exp ^a	2.40×10^{-5}	—	—

^a The experimental value for the self-diffusion coefficient of water is extrapolated from the corresponding values measured at different temperatures and reported in ref. 58.

hydrogen bonds at the interfacial region, as well as the decay of the average radial density profiles discussed in Fig. 6, are also consistent with predictions obtained by classical density-functional theory on confined associating fluids.⁵⁷

Finally, in Table 2 the water self-diffusion coefficients are reported for all the simulated systems. While the previously discussed results on ensemble averages of structural properties were little sensitive to the adopted solvent models, a slightly larger variability is found in semi-dynamic properties such as the diffusion coefficients. In fact, the calculated coefficients for the S, M, and L systems with the different solvent models range from 7.51×10^{-6} to 1.04×10^{-7} cm² s⁻¹, with an observed trend AA > 2BDS > 3BDS for the S and M systems, and no clear trend across the considered system size. The calculated coefficients are on the other hand always at least one order of magnitude smaller than the bulk TIP3P one (2.57×10^{-5} cm² s⁻¹), which compares very well with the reported experimental value (2.40×10^{-5} cm² s⁻¹). While the number of simulation setups considered in this work is too limited to meaningfully discuss trends across the considered RM sizes and solvent models, on the whole these results suggest a hampering effect on the diffusion properties of water when confined.

4 Conclusions

In this article, we investigate the structural and dynamical properties of water confined in three differently sized RMs constituted by the nonionic surfactant molecules of Span 80 dispersed in an oil phase of cyclohexane. The three RMs considered have a number of Span 80 molecules equal to 51, 246, and 475, respectively, and have an average inner-core water radius in the range of 10–60 Å. The cyclohexane solvent was modeled through both an AA and a CG approach, to assess the effect of coarse-graining of the solvent on the calculated properties of confined water.

Our results show that the three RMs have quasi-spherical shape with minor fluctuations and sphericity degree increasing with increasing RM size, and further highlight for each RM the presence of two distinct regions of water featuring different structural and dynamical properties as a consequence of confinement. In particular, the RMs show an inner region of bulk-like water and an interfacial region where the water features a

lower density, a lower tetrahedral packing, a slightly lower number of hydrogen bonds, and a smaller self-diffusion coefficient with respect to bulk water. The spatial extent of the two regions depends on the size of the systems considered and can be inferred from the analysis of the average radial density profile of the water inside the RMs. In particular, for the considered S, M, and L RMs, bulk water is found in an approximately spherical region of radius 3.5, 20, and 35 Å, respectively, after which the average radial density decays and vanishes at about 20, 40 and 55 Å, respectively.

Our work also shows that the solvent can be safely modeled by a CG approach with negligible effect on the reproducibility of the properties of confined water and a huge saving in computational resources, thus unlocking the possibility of simulating larger RMs or more complex systems that involve reactions occurring in the RMs or in the presence of spectroscopically active molecular probes.

Conflicts of interest

There are no conflicts to declare.

Data availability

The input files for the MD simulations reported in this work have been included as part of the SI in the form of .pdb, .psf, .par, and NAMD configuration files. See DOI: <https://doi.org/10.1039/d5cp02542g>

Acknowledgements

Computational work has been carried out on the C3P (Computational Chemistry Community in Padua) HPC facility of the Department of Chemical Sciences of the University of Padua. This work has been also partially supported by the Spoke 1 “FutureHPC & BigData” of the Italian Research Center on High-Performance Computing, Big Data and Quantum Computing (ICSC) funded by MUR Missione 4 – Next Generation EU (NGEU).

Notes and references

- H. K. Christenson, *J. Phys.: Condens. Matter*, 2001, **13**, R95–R133.
- N. Giovambattista, P. J. Rossky and P. G. Debenedetti, *Annu. Rev. Phys. Chem.*, 2012, **63**, 179–200.
- G. A. Mansoori and S. A. Rice, *Advances in Chemical Physics*, John Wiley & Sons, Ltd, 2014, ch. 5, vol. 156, pp. 197–294.
- S. Cervený, F. Mallamace, J. Swenson, M. Vogel and L. Xu, *Chem. Rev.*, 2016, **116**, 7608–7625.
- S. Chakraborty, H. Kumar, C. Dasgupta and P. K. Maiti, *Acc. Chem. Res.*, 2017, **50**, 2139–2146.
- B. Malfait, A. Jani, J. B. Mietner, R. Lefort, P. Huber, M. Fröba and D. Morineau, *J. Phys. Chem. C*, 2021, **125**, 16864–16874.



- 7 A. Jani, M. Busch, J. B. Mietner, J. Ollivier, M. Appel, B. Frick, J.-M. Zanotti, A. Ghoufi, P. Huber, M. Fröba and D. Morineau, *J. Chem. Phys.*, 2021, **154**, 094505.
- 8 B. Malfait, A. Moréac, A. Jani, R. Lefort, P. Huber, M. Fröba and D. Morineau, *J. Phys. Chem. C*, 2022, **126**, 3520–3531.
- 9 N. C. Gießelmann, P. Lenz, S.-M. Meinert, T. Simon, W. Jo, N. N. Striker, M. Fröba and F. Lehmkuhler, *J. Phys. Chem. C*, 2024, **128**, 499–507.
- 10 T. C. V. Haug, F. Hoffmann, M. N. Tasova, R. Heffels and M. Fröba, *Adv. Mater. Interfaces*, 2025, **12**, 2400847.
- 11 A. Antonello, G. Jakob, P. Dolcet, R. Momper, M. Kokkinopoulou, K. Landfester, R. Muñoz Espí and S. Gross, *Chem. Mater.*, 2017, **29**, 985–997.
- 12 M. Foroutan, S. M. Fatemi and F. Esmailian, *Eur. Phys. J. E*, 2017, **40**, 19.
- 13 A. Amani, P. York, H. de Waard and J. Anwar, *Soft Matter*, 2011, **7**, 2900–2908.
- 14 S.-S. Qin, Y.-X. Yu, Q.-K. Li and Z.-W. Yu, *Biochemistry*, 2013, **52**, 1477–1489.
- 15 A. Catte and V. S. Oganesyan, *Phys. Chem. Chem. Phys.*, 2025, **27**, 4775–4784.
- 16 J. Faeder and B. M. Ladanyi, *J. Phys. Chem. B*, 2000, **104**, 1033–1046.
- 17 J. Faeder, M. V. Albert and B. M. Ladanyi, *Langmuir*, 2003, **19**, 2514–2520.
- 18 S. Senapati and M. L. Berkowitz, *J. Phys. Chem. B*, 2003, **107**, 12906–12916.
- 19 S. Abel, F. Sterpone, S. Bandyopadhyay and M. Marchi, *J. Phys. Chem. B*, 2004, **108**, 19458–19466.
- 20 M. R. Harpham, B. M. Ladanyi and N. E. Levinger, *J. Phys. Chem. B*, 2005, **109**, 16891–16900.
- 21 S. Abel, M. Waks, M. Marchi and W. Urbach, *Langmuir*, 2006, **22**, 9112–9120.
- 22 V. R. Vasquez, B. C. Williams and O. A. Graeve, *J. Phys. Chem. B*, 2011, **115**, 2979–2987.
- 23 V. R. Hande and S. Chakrabarty, *Phys. Chem. Chem. Phys.*, 2016, **18**, 21767–21779.
- 24 K. Landfester, *Annu. Rev. Mater. Res.*, 2006, **36**, 231–279.
- 25 H.-X. Zhou, *Arch. Biochem. Biophys.*, 2008, **469**, 76–82.
- 26 M. Lechuga, M. Fernández-Serrano, E. Jurado, J. Núñez Olea and F. Ríos, *Ecotoxicol. Environ. Saf.*, 2016, **125**, 1–8.
- 27 C. Prieto and L. Calvo, *J. Appl. Chem.*, 2013, **2013**, 930356.
- 28 O. V. Borisov, J. A. Ji and Y. John Wang, *J. Pharm. Sci.*, 2015, **104**, 1005–1018.
- 29 M. Mannoor, S. Kang and Y. K. Suh, *Adv. Condens. Matter Phys.*, 2015, **2015**, 739458.
- 30 I. V. Kopanichuk, E. A. Vedenchuk, A. S. Koneva and A. A. Vanin, *J. Phys. Chem. B*, 2018, **122**, 8047–8055.
- 31 Y. Ono, T. Mizuguchi and M. Fukuyama, *Trans. Jap. Soc. Simul. Technol.*, 2023, **15**, 36–41.
- 32 M. Fukuyama, T. Mizuguchi, P. Santivongskul, Y. Ono, M. Kasuya, A. Inagawa and A. Hibara, *Nanoscale*, 2024, **16**, 4056–4062.
- 33 A. Amani, P. York, H. de Waard and J. Anwar, *Soft Matter*, 2011, **7**, 2900–2908.
- 34 A. V. Sangwai and R. Sureshkumar, *Langmuir*, 2011, **27**, 6628–6638.
- 35 S. J. Marrink, A. H. de Vries and A. E. Mark, *J. Phys. Chem. B*, 2004, **108**, 750–760.
- 36 S. J. Marrink, H. J. Risselada, S. Yefimov, D. P. Tieleman and A. H. de Vries, *J. Phys. Chem. B*, 2007, **111**, 7812–7824.
- 37 L. Martínez, R. Andrade, E. G. Birgin and J. M. Martínez, *J. Comput. Chem.*, 2009, **30**, 2157–2164.
- 38 A. Maitra, *J. Phys. Chem.*, 1984, **88**, 5122–5125.
- 39 A. Amararene, M. Gindre, J.-Y. Le Huérou, W. Urbach, D. Valdez and M. Waks, *Phys. Rev. E: Stat. Phys., Plasmas, Fluids, Relat. Interdiscip. Top.*, 2000, **61**, 682–689.
- 40 G. Eskici and P. H. Axelsen, *J. Phys. Chem. B*, 2016, **120**, 11337–11347.
- 41 O. M. Szklarczyk, S. J. Bachmann and W. F. van Gunsteren, *J. Comput. Chem.*, 2014, **35**, 789–801.
- 42 O. M. Szklarczyk, E. Arvaniti and W. F. van Gunsteren, *J. Comput. Chem.*, 2015, **36**, 1311–1321.
- 43 J. C. Phillips, R. Braun, W. Wang, J. Gumbart, E. Tajkhorshid, E. Villa, C. Chipot, R. D. Skeel, L. Kalé and K. Schulten, *J. Comput. Chem.*, 2005, **26**, 1781–1802.
- 44 B. R. Brooks, R. E. Bruccoleri, B. D. Olafson, D. J. States, S. Swaminathan and M. Karplus, *J. Comput. Chem.*, 1983, **4**, 187–217.
- 45 B. R. Brooks, C. L. Brooks III, A. D. Mackerell Jr., L. Nilsson, R. J. Petrella, B. Roux, Y. Won, G. Archontis, C. Bartels, S. Boresch, A. Caffisch, L. Caves, Q. Cui, A. R. Dinner, M. Feig, S. Fischer, J. Gao, M. Hodoscek, W. Im, K. Kuczera, T. Lazaridis, J. Ma, V. Ovchinnikov, E. Paci, R. W. Pastor, C. B. Post, J. Z. Pu, M. Schaefer, B. Tidor, R. M. Venable, H. L. Woodcock, X. Wu, W. Yang, D. M. York and M. Karplus, *J. Comput. Chem.*, 2009, **30**, 1545–1614.
- 46 S. Jo, T. Kim, V. G. Iyer and W. Im, *J. Comput. Chem.*, 2008, **29**, 1859–1865.
- 47 E. Núñez Rojas and H. Domínguez, *Rev. Mex. Fis.*, 2013, **59**, 530–539.
- 48 S. Han, *Bull. Korean Chem. Soc.*, 2013, **34**, 946–948.
- 49 W. L. Jorgensen, J. Chandrasekhar, J. D. Madura, R. W. Impey and M. L. Klein, *J. Chem. Phys.*, 1983, **79**, 926–935.
- 50 W. Humphrey, A. Dalke and K. Schulten, *J. Mol. Graphics*, 1996, **14**, 33–38.
- 51 P.-L. Chau and A. J. Hardwick, *Mol. Phys.*, 1998, **93**, 511–518.
- 52 J. R. Errington and P. G. Debenedetti, *Nature*, 2001, **409**, 318–321.
- 53 V. R. Hande and S. Chakrabarty, *J. Phys. Chem. B*, 2015, **119**, 11346–11357.
- 54 B. Shadrack Jabes, R. Klein and L. Delle Site, *Adv. Theory Simul.*, 2018, **1**, 1800025.
- 55 M. Ferrario, M. Haughney, I. R. McDonald and M. L. Klein, *J. Chem. Phys.*, 1990, **93**, 5156–5166.
- 56 M. P. Allen and D. J. Tildesley, *Computer Simulation of Liquids*, Oxford University Press, Oxford, 2017.
- 57 Y.-X. Yu and J. Wu, *J. Chem. Phys.*, 2002, **116**, 7094–7103.
- 58 M. Holz, S. R. Heil and A. Sacco, *Phys. Chem. Chem. Phys.*, 2000, **2**, 4740–4742.

